NACA

RESEARCH MEMORANDUM

HEAT TRANSFER ON THE LIFTING SURFACES OF A 60° DELTA

WING AT ANGLE OF ATTACK FOR MACH NUMBER 1.98

By Howard S. Carter

Langley Aeronautical Laboratory
Langley Field, Va.

NATIONAL ADVISORY COMMITTEE
FOR AERONAUTICS
WASHINGTON
May 31, 1956
Declassified January 12, 1961

NATIONAL ADVISORY COMMITTEE FOR AERONAUTICS

RESEARCH MEMORANDUM

HEAT TRANSFER ON THE LIFTING SURFACES OF A 60° DELTA

WING AT ANGLE OF ATTACK FOR MACH NUMBER 1.98

By Howard S. Carter

SUMMARY

The heat transfer and pressures on the lifting surfaces of a 60° delta wing with NACA 65A005 profile are presented for angles of attack up to 9°. The tests were made under steady flow conditions in a free jet at a Mach number of 1.98 and for a Reynolds number based on the mean aerodynamic chord of 22×10^6.

The heat transfer on the lower surface of the wing was within 9 percent of values obtained by flat-plate theory for all angles of attack up to 9°. The heat transfer on the upper surface disagreed progressively more with flat-plate theory as angle of attack increased until it was about 30 percent less than theory at an angle of attack of 9°. The pressures on the surfaces of the wing indicated that, at all angles of attack of the tests, spanwise flow components existed in the flow over the wing.

INTRODUCTION

Most of the existing theories of convective heat transfer at high speed (for example, refs. 1, 2, and 3) apply directly to boundary layers in which there are no pressure nor temperature gradients along the surface. In order to apply these theories, local flow conditions must be known. The convective heat transfer through the boundary layer of flat plates, wedges, cones, and cylinders can usually be predicted fairly accurately with these theories or with modifications of these theories (ref. 4). However, these theories may not be adequate to approximate the heat transfer on surfaces which do have pressure and temperature gradients, shock formations, crossflows in the boundary layer, or other phenomena that can influence accurate calculation of the local conditions. For example, a delta wing at zero angle of attack may have these factors affecting the local conditions, and hence influencing both theoretical

and experimental values of heat transfer. As the angle of attack of a delta wing is increased, these factors affecting the local conditions and hence the heat transfer may vary considerably.

Most of the high-speed airplanes and missiles being developed at present are using wings, stabilizers, or fins that have sweptback leading edges. It is becoming more needful that the heat-transfer characteristics on the lifting surfaces of this type of airfoil be investigated. Hence, the Pilotless Aircraft Research Division of the Langley Aeronautical Laboratory has included in its heat-transfer program an experimental investigation to determine the heat-transfer characteristics of a 60° delta wing for various angles of attack at a Mach number of 1.98. In order to determine the local flow conditions, the pressures were measured at the same stations as the temperatures. The tests were conducted in the preflight jet test facility located at Wallops Island, Va.

SYMBOLS

α angle of attack, deg

c_w specific heat of skin, Btu/lb-$^\circ$F

N_{St} local Stanton number, $\dfrac{h}{c_p \rho_l V_l}$

C_p pressure coefficient, $\dfrac{p_l - p_\infty}{q_\infty}$

c_p specific heat of air at constant pressure, Btu/lb-$^\circ$F

c_r wing chord at the root, ft

ρ_w mass density of skin, lb/cu ft

ρ_l local density of air, lb/cu ft

h local aerodynamic heat-transfer coefficient, Btu/sec-sq ft-$^\circ$F

p_l local static pressure, lb/sq ft

p_∞ free-stream static pressure, lb/sq ft

q_∞ free-stream dynamic pressure, lb/sq ft

t skin thickness, ft

τ time, sec

T_{aw} adiabatic wall temperature, ^oR

$T_{t,\infty}$ free-stream stagnation temperature, ^oR

T_l local static temperature, ^oR

T_w wall temperature, ^oR

V_∞ free-stream velocity, ft/sec

V_l local velocity, ft/sec

M Mach number

APPARATUS

Test Facility

The investigation reported herein was conducted in the preflight jet test facility located at the Pilotless Aircraft Research Station at Wallops Island, Va. This jet, which is a blowdown type, is described in reference 5 except that, for these tests, a 27- by 27-inch nozzle was used.

A photograph of the semispan wing mounted at the exit of the 27- by 27-inch nozzle is shown in figure 1. The most forward tip of the wing was positioned 5 inches upstream of the nozzle exit and 6 inches above the bottom plate of the nozzle. As shown in the photograph, the wing assembly was mounted on a turntable which could be adjusted for an angle-of-attack range from 0° to 10°. Not shown in the photograph but mounted on top of the 27- by 27-inch nozzle was a retractable clamping arm which was used to steady the wing during the highly turbulent transient flow conditions at the beginning and ending of each blowdown test.

Model

A drawing of the 60° delta semispan wing model showing the geometry and instrumentation is shown in figure 2. This wing had a mean aerodynamic chord of 1.56 feet and a plan-form area of the model of 1.57 square feet. The streamwise airfoil section was NACA 65A005.

As shown in the side view and sectional view of the wing, the spars were spaced so as to leave several large open bays over which the skin (0.050 inch thick) was isolated from large heat sinks. To further isolate the skin from the other wing structure, a sheet of 1/16-inch-thick plastic was placed under the skin. The skin made contact with the other structure of the wing through rivets and at its extreme edges. The wing was mounted on a flat deflector plate as shown in figure 2. The plate had a 45° swept leading edge and was beveled on the bottom of all edges except the trailing edge. This plate isolated the wing from any disturbances originating from the supporting strut. The leading edge, trailing edge, and skin of the wing were made of Invar steel. Invar steel, which has a small coefficient of expansion, was used for these wing portions which were exposed to the airstream in order to minimize the internal stresses and distortions caused by a hot surface and a relatively cool interior structure. The spars, deflector plate, and wing supporting structure were made of low carbon steel.

The wing had 12 static-pressure orifices (0.0625-inch diameter) on one surface and 12 thermocouples (0.01-inch diameter, iron-constantan) exactly opposite on the other surface. Each of these orifices and thermocouples was placed in the skin near the center of an open bay; since, at these points, the skin was more nearly isolated from the rest of the structure. In addition, in order to permit the heat conduction along the wing and into the other wing structure to be determined, several other thermocouples were mounted on the skin near the edge of the open bays and several were mounted on the inside structure halfway between the two surfaces of the wing.

At the top of figure 2 is a cross-sectional view of a section of the wing which shows a typical orifice and thermocouple installation in one of the bays. The thermocouples on the skin were welded to the inside surface. The temperature gradient through the thickness of the skin was calculated and found to be negligible.

TESTS AND PROCEDURE

Range of Variables

The semispan model of the 60° delta wing was tested in a vertical position as shown in figure 1. However, to simplify the presentation of the data and to help in visualization of the results, the wing is treated as though it were in the horizontal plane. Tests were made at a Mach number of 1.98 and at angles of attack of 0°, 3°, 6°, and 9°. The wing was instrumented to measure pressures on one surface and temperatures on the other. However, the data are presented in such manner as to show both upper- and lower-surface effects on the same figure. Temperature and static pressure on the wing, free-stream total pressure, and free-stream total temperature were measured continually during each test. All measurements were time correlated by oscillograph recorders.

At the beginning of each blowdown test, the clamping arm was in position to grip the wing near the outer tip in order to keep the wing steady during the transient period of the test. This was necessary to insure that the wing did not buffet to destruction as a result of the extreme turbulent flow during this part of the test. After approximately 2 seconds, the flow became steady, and the arm was withdrawn from the vicinity of the wing.

The test then continued at sea-level free-stream conditions for approximately 8 seconds, after which time the free-stream total pressure could not be maintained due to the exhaustion of the air from the storage spheres.

Reduction of Data

The heat-transfer parameters as presented herein are based on local flow conditions. The flow at all measuring stations for all tests was assumed to be turbulent, since the lowest local Reynolds number calculated for any station was about 4×10^6. Reference 6 shows that turbulent flow is usually established at about a Reynolds number of 3×10^6 for $M = 1.98$. The values of heat-transfer parameters obtained verified that the flow was turbulent.

The aerodynamic heat-transfer coefficients were calculated from data measured during the transient heating of the wing after the establishment of steady air flow from the nozzle. Radiation from the wing surface, conduction into the internal structure, and conduction along the surface were found to be negligible. If these terms are negligible, the convective heat transferred to the model can be equated to the heat

absorbed by the model skin per unit of time. This relation is expressed
in the following equation:

$$h(T_{aw} - T_w) = \rho_w c_w t \frac{dT_w}{d\tau}$$

The aerodynamic heat-transfer coefficient h was evaluated by using the
mass density ρ_w of the Invar skin as 502.5 lb/cu ft and its specific
heat c_w as given in figure 3. The specific heat of Invar presented in
this figure was obtained from tests performed in the Instrument Research
Division of the Langley Laboratory. The skin thickness t at the
thermocouple stations was 0.050 inch. The adiabatic wall temperature
was obtained from the following equation:

$$T_{aw} = N_{Pr}^{1/3}\left(T_{t,\infty} - T_l\right) + T_l$$

in which $N_{Pr}^{1/3}$ is the theoretical temperature-recovery factor for
turbulent convective heat transfer as based on wall temperature. Exper-
imental temperature-recovery factors were not obtained from these tests
since the skin temperature did not reach equilibrium.

The skin temperature and its time rate of change were obtained from
the measured time histories of the skin temperature. A typical skin
temperature and stagnation-temperature time history is shown in figure 4.
This figure shows that, during each blowdown test and especially at the
beginning of each test, the time rate of change of wall temperature
$dT_w/d\tau$ and the temperature forcing function $T_{aw} - T_w$ were both of
large magnitude. Hence, an error in wall temperature or in the temper-
ature time derivative would not affect the heat-transfer coefficient to
any great extent. From consideration of all known influencing factors,
the accuracy of the heat-transfer data is believed to be approximately
10 percent.

Shadowgraphs of the wing as it was tested at zero angle of attack
showed that the bow wave ahead of the wing leading edge had essentially
the same slope as the leading edge. The free-stream Mach number normal
to this bow wave was approximately unity. Hence, it was assumed that
the loss in total pressure across this bow wave was negligible and that
local total pressures were equal to free-stream total pressure. There
may, however, have been some other shocks along the upper surface of
the wing at angles of attack greater than zero which may have caused a
considerable difference between local and free-stream total pressures.
Reference 7, which concerns a test of a somewhat similar wing, showed
that at moderate angles of attack a lambda shock existed on the upper
surface near the leading edge.

Pressure Measurements

The variation of pressure coefficient with angle of attack for the three semispan stations on the wing surfaces is presented in figure 5. In this figure, the symbols used to identify the data points are also shown superimposed over their respective stations on a sketch of the wing. The pressure coefficient is plotted in this manner to show its continuous variation through zero angle of attack and also better to compare effects of angle of attack on the upper and lower surfaces. This figure shows that the pressure variation with angle of attack is slightly greater on the lower surface.

The chordwise and spanwise variations of pressure coefficient are presented in figures 6 and 7, respectively, for four angles of attack. Figure 6 shows that, in general, the pressures on the wing surfaces decreased for all angles of attack as the flow progressed toward the trailing edge. Likewise, figure 7 shows that the pressures on the wing surface, for all angles of attack tested, were progressively less as the measurement station approached the tip. Figure 7 indicates also that, at angle of attack, these spanwise pressure gradients were more pronounced on the upper surface. The pressure gradients in these two figures just presented indicate that the air flow over the surface of the wing turned toward the wing tip. Reference 7, which concerns a test of a somewhat similar wing to the one reported herein, shows that at an angle of attack of 9° the flow on the upper surface at $0.70c_r$ and at 65-percent local semispan turned approximately 14° toward the tip. The 60° delta wing reported on in this paper and also the testing conditions were sufficiently different from those of reference 7 to preclude any direct comparison other than general trends in the flow patterns.

Heat Transfer

In order to show the values and trends of the actual heating effects, the heat-transfer coefficient is presented first (figs. 8 to 10). Then, in order to provide a comparison of the heating characteristics of this wing with theory, the Stanton number is presented (figs. 11 to 13). The variations in heat-transfer parameters with temperature ratio T_w/T_l predicted by Van Driest flat-plate theory could not be determined, since the scatter of the data was greater than the temperature effect. Hence, all heat-transfer coefficients and Stanton numbers are presented for a temperature ratio T_w/T_l of 1.4 only.

Heat-transfer coefficient.- The variation of heat-transfer coefficient with angle of attack for the 12 measuring stations is shown in figure 8. The symbols used to define the curves are also shown superimposed over their respective stations on a sketch of the wing. The heat-transfer coefficient is plotted in this manner to show its continuity at zero angle of attack and better to compare the effect of angle of attack on the two surfaces. The heat-transfer coefficient decreased on the upper surface and increased on the lower as angle of attack increased.

The chordwise and spanwise variations of heat-transfer coefficient are presented in figures 9 and 10, respectively, for four angles of attack. Figure 9 shows that the heat-transfer coefficient decreased for all angles of attack as the flow progressed toward the trailing edge. In figure 10, the two stations nearer the tip at 0.84 root chord show a larger change of heat-transfer coefficient with angle of attack than the inboard station.

Stanton number.- The variation of Stanton number with angle of attack for the 12 measuring stations is presented in figure 11. The symbols used to define the curves are again shown superimposed over their respective stations on a sketch of the wing. The Stanton number is plotted in this manner to show its continuity at zero angle of attack and to separate the data for the two surfaces. The Stanton number on the lower surface was essentially constant for angles of attack up to 9°. On the upper surface, however, the Stanton number decreased as angle of attack increased. At an angle of attack of 9°, the Stanton number on the upper surface had decreased approximately 30 percent below the value for zero angle of attack.

Figure 12 presents the chordwise variation of Stanton number for four angles of attack. The Stanton number on the lower surface did not vary appreciably with angle of attack. Hence, only one curve was faired through the lower-surface data. Added to each part of this figure is a Van Driest turbulent-theory (ref. 3) curve for a flat plate based on local conditions. This theory was modified as suggested in reference 8. This theory predicted that the local Stanton numbers at the measuring stations on this wing would be constant for all angles of attack. On the lower surface, the Stanton numbers were in good agreement with theory for the 15-percent and 35-percent semispan stations; whereas the data were about 9 percent lower than theory for the 54-percent semispan station. On the upper surface, the Stanton number for all three semispan stations disagreed progressively more with theory as the angle of attack increased. At 9° angle of attack, the experimental data on the upper-surface stations were about 30 percent less than theory.

The reduction of Stanton number on the upper surface at angles of attack may have been caused in part to the existence of shock waves near the leading edge of the upper surface such as are shown to exist on a somewhat similar wing in reference 7. These shocks, if they did exist,

could cause disturbances in the boundary-layer flow which would make the heat transfer unpredictable by present theories. Hence, the theoretical curves as presented may be considerably in error for the upper surface. These shock waves could also cause an error in the reduction of the data. The assumption that local-stream total pressure was equal to free-stream total pressure may have been more in error on the upper surface as the angle of attack increased.

The spanwise variation of Stanton number at 0.84 root chord is presented in figure 13 for the four angles of attack. A Van Driest turbulent theory curve for a flat plate based on local conditions is shown on this figure by a dashed curve. The faired experimental values of Stanton number are all less than theory at this 0.84 root chord station, varying from slightly less for an angle of attack of 9° on the lower surface to about 30 percent less at an angle of attack of 9° on the upper surface. This figure also shows that the spanwise variation in Stanton number at this 0.84 root chord station was less than that predicted by theory. This difference from theory may have been due in part to such phenomena as spanwise components in the boundary-layer flow, thickening of the boundary layer toward the tip, and erroneous Reynolds number calculations resulting from lack of information on the path of air flow.

CONCLUSIONS

From an experimental investigation in a free jet to determine the heat transfer on the lifting surfaces of a 60° delta wing at angle of attack for Mach number of 1.98, the following conclusions can be made:

1. At angles of attack up to 9°, the Stanton number on the lower surface was in good agreement with theory for the 15-percent and 35-percent semispan stations and was about 9 percent less than theory for the 54-percent semispan station.

2. As angle of attack increased from 0° to 9°, the Stanton number at all measuring stations on the upper surface disagreed progressively more with theory, being about 30 percent less than theory at 9° angle of attack.

3. The spanwise variation of Stanton number along the 0.84 root chord station was less than that predicted by theory.

4. The pressures on the surface of the wing indicated that, at all angles of attack of the tests, spanwise components existed in the flow over the wing.

Langley Aeronautical Laboratory,
    National Advisory Committee for Aeronautics,
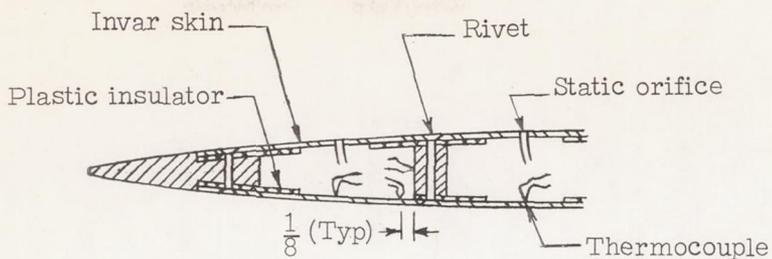   Langley Field, Va., March 6, 1956.

REFERENCES

1. Van Driest, E. R.: Investigation of Laminar Boundary Layer in
     Compressible Fluids Using the Crocco Method. NACA TN 2597, 1952.

2. Klunker, E. B., and McLean, F. Edward: Laminar Friction and Heat
     Transfer at Mach Numbers From 1 to 10. NACA TN 2499, 1951.

3. Van Driest, E. R.: Turbulent Boundary Layer in Compressible Fluids.
     Jour. Aero. Sci., vol. 18, no. 3, Mar. 1951, pp. 145-160, 216.

4. Eckert, Ernst R. G.: Survey on Heat Transfer at High Speeds. WADC Tech.
     Rep. 54-70, Wright Air Dev. Center, U. S. Air Force, Apr. 1954.

5. Faget, Maxime A., Watson, Raymond S., and Bartlett, Walter A., Jr.:
     Free-Jet Tests of a 6.5-Inch-Diameter Ram-Jet Engine at Mach
     Numbers of 1.81 and 2.00. NACA RM L50L06, 1951.

6. Rubesin, Morris W., Rumsey, Charles B., and Varga, Steven A.: A
     Summary of Available Knowledge Concerning Skin Friction and Heat
     Transfer and Its Application to the Design of High-Speed Missiles.
     NACA RM A51J25a, 1951.

7. Hatch, John E., Jr., and Gallagher, James J.: Aerodynamic Charac-
     teristics of a 68.4° Delta Wing at Mach Numbers of 1.6 and 1.9
     Over a Wide Reynolds Number Range. NACA RM L53I08, 1953.

8. Van Driest, E. R.: The Turbulent Boundary Layer With Variable
     Prandtl Number. Rep. No. AL-1914, North American Aviation, Inc.,
     Apr. 2, 1954.
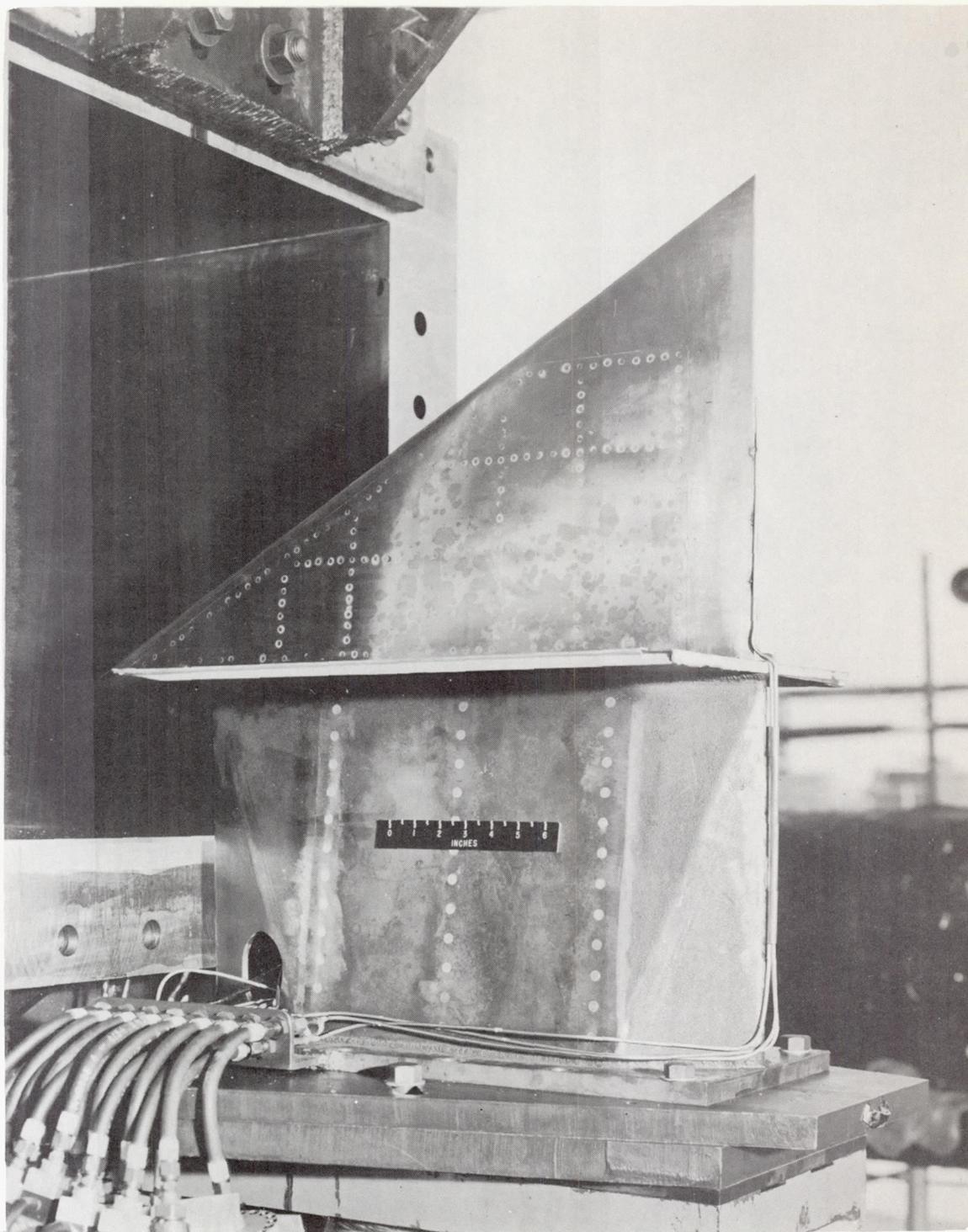
L-90403

Figure 1.- Photograph of the wing mounted in the preflight-jet test
facility.

Invar skin

Rivet

Plastic insulator

Static orifice

$\frac{1}{8}$ (Typ)

Thermocouple

Section A---A (Enlarged)

45°

Deflector plate

7.40

16.15

3.10

A

A

.3.25

60°

2.40

8.5   3.0   3.0   3.0   3.0   3.0   4.5

28.0
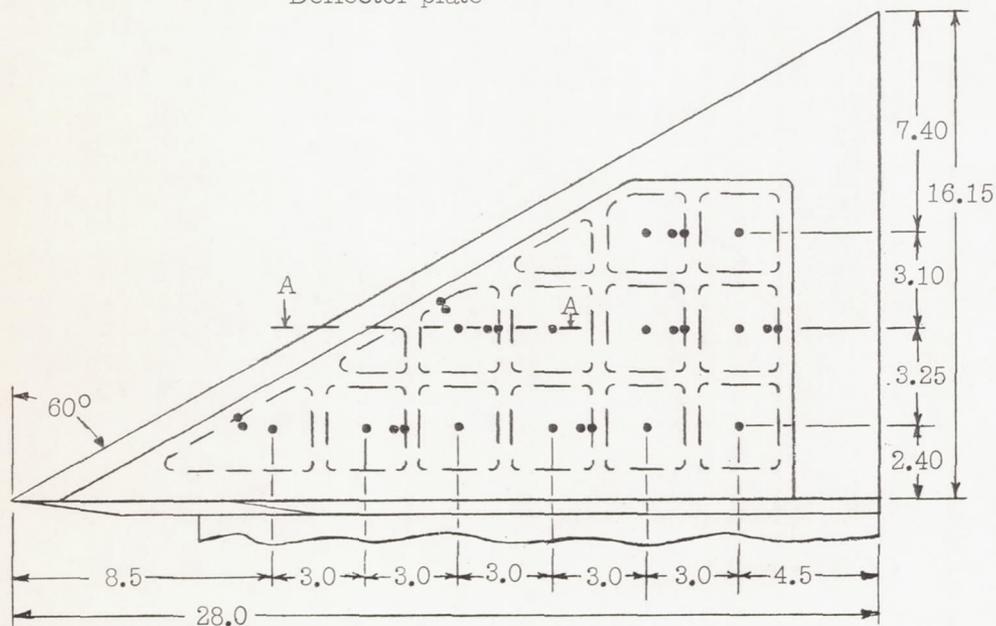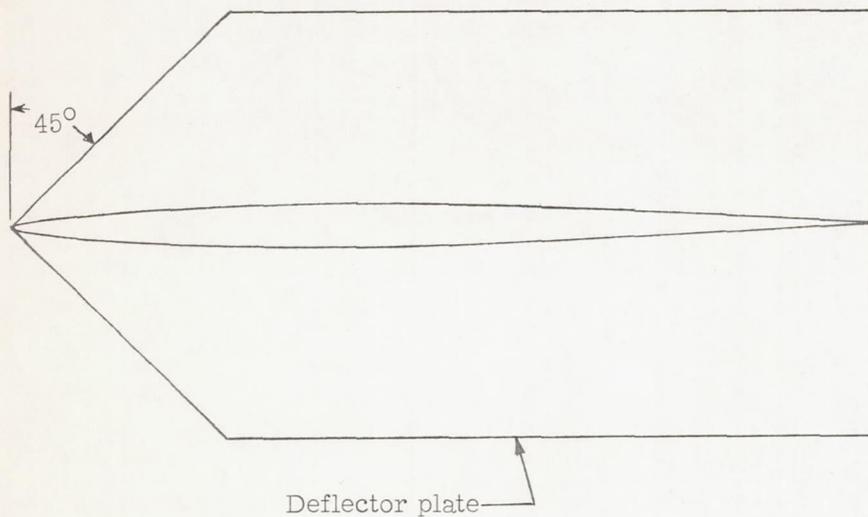
Figure 2.- Drawing of the 60° delta wing showing construction and instru-
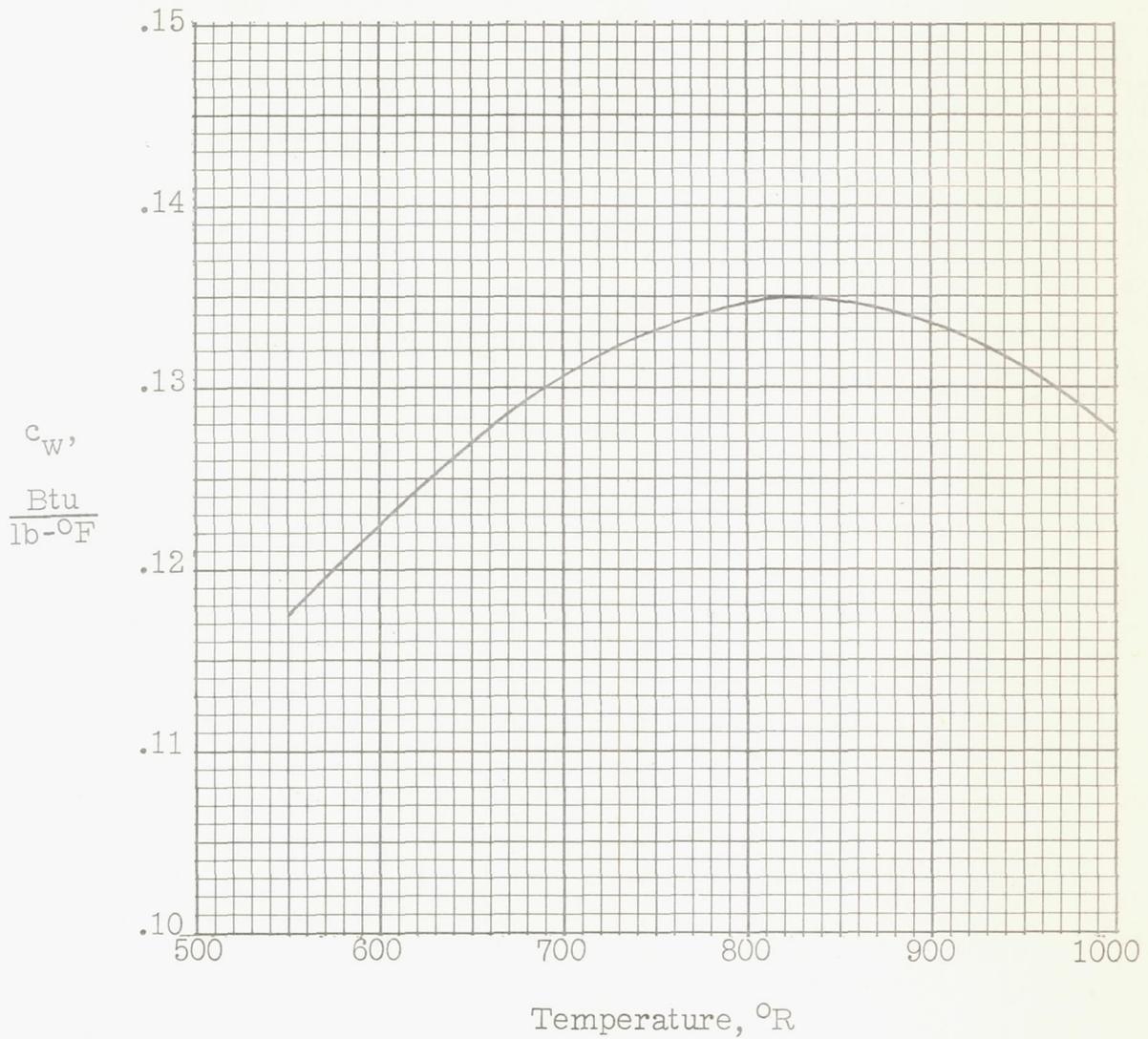mentation. All dimensions are in inches.
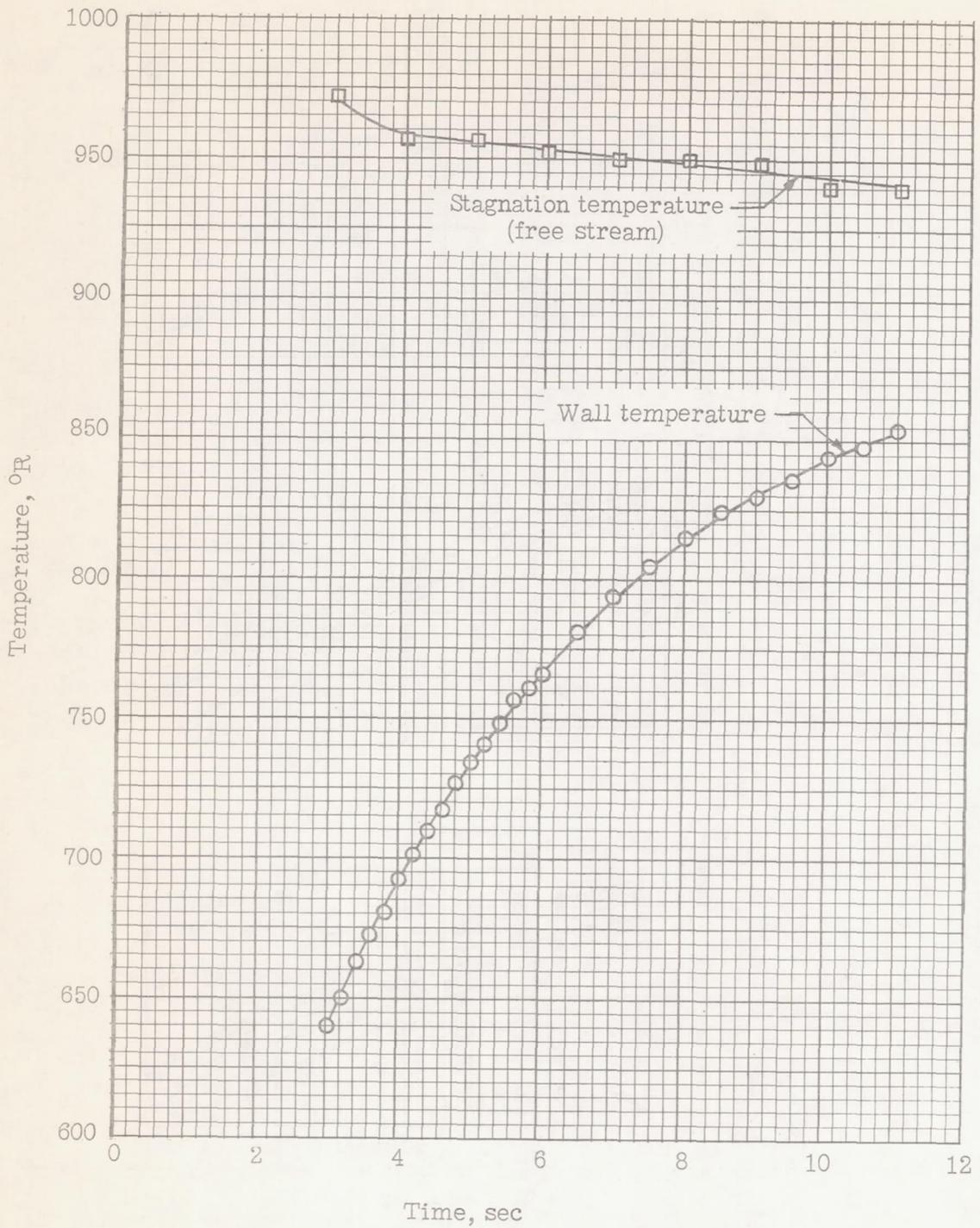
Figure 3.- Variation of the specific heat of Invar with temperature.

Figure 4.- Typical temperature-time curves for wall temperature and free-stream stagnation temperature.
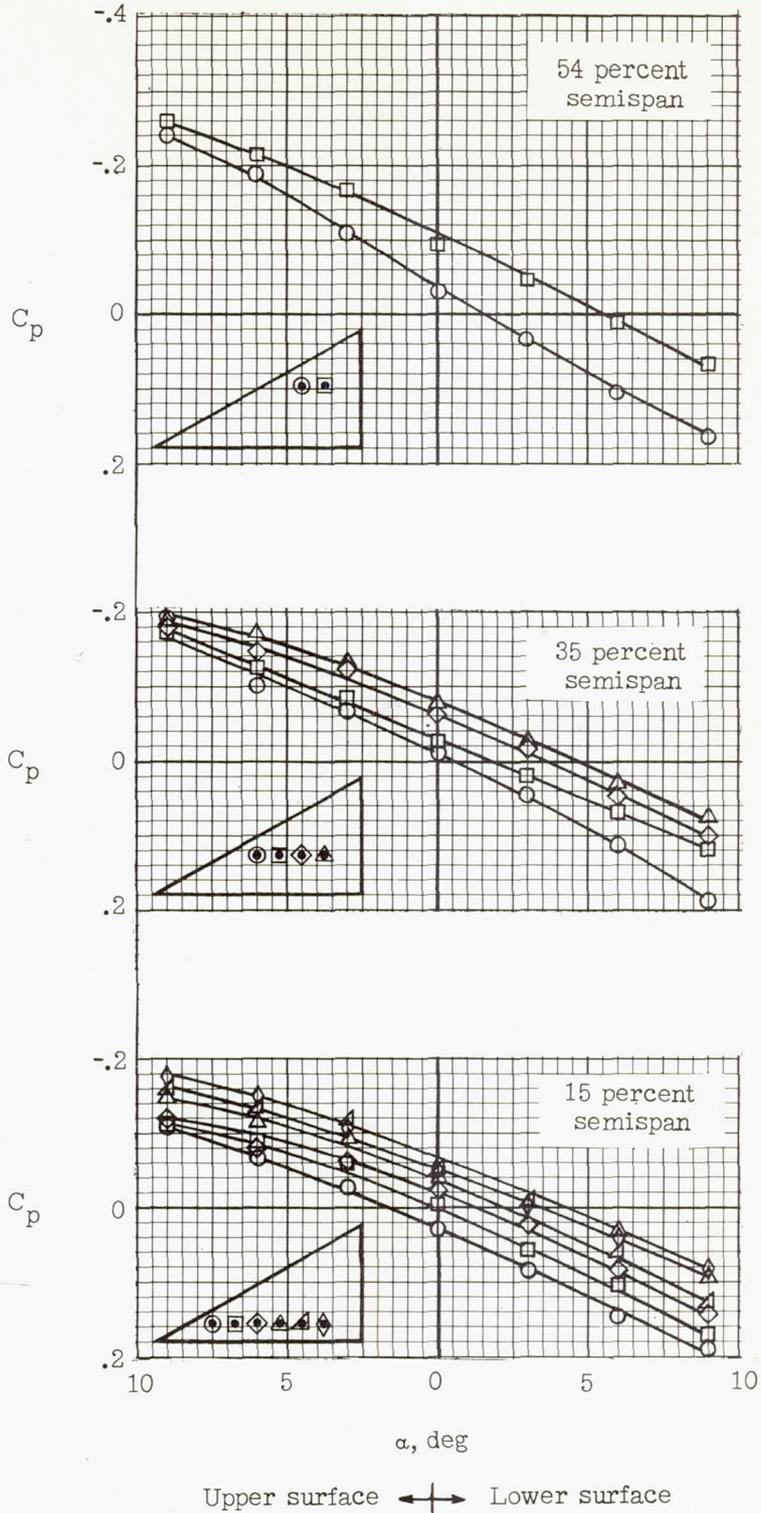
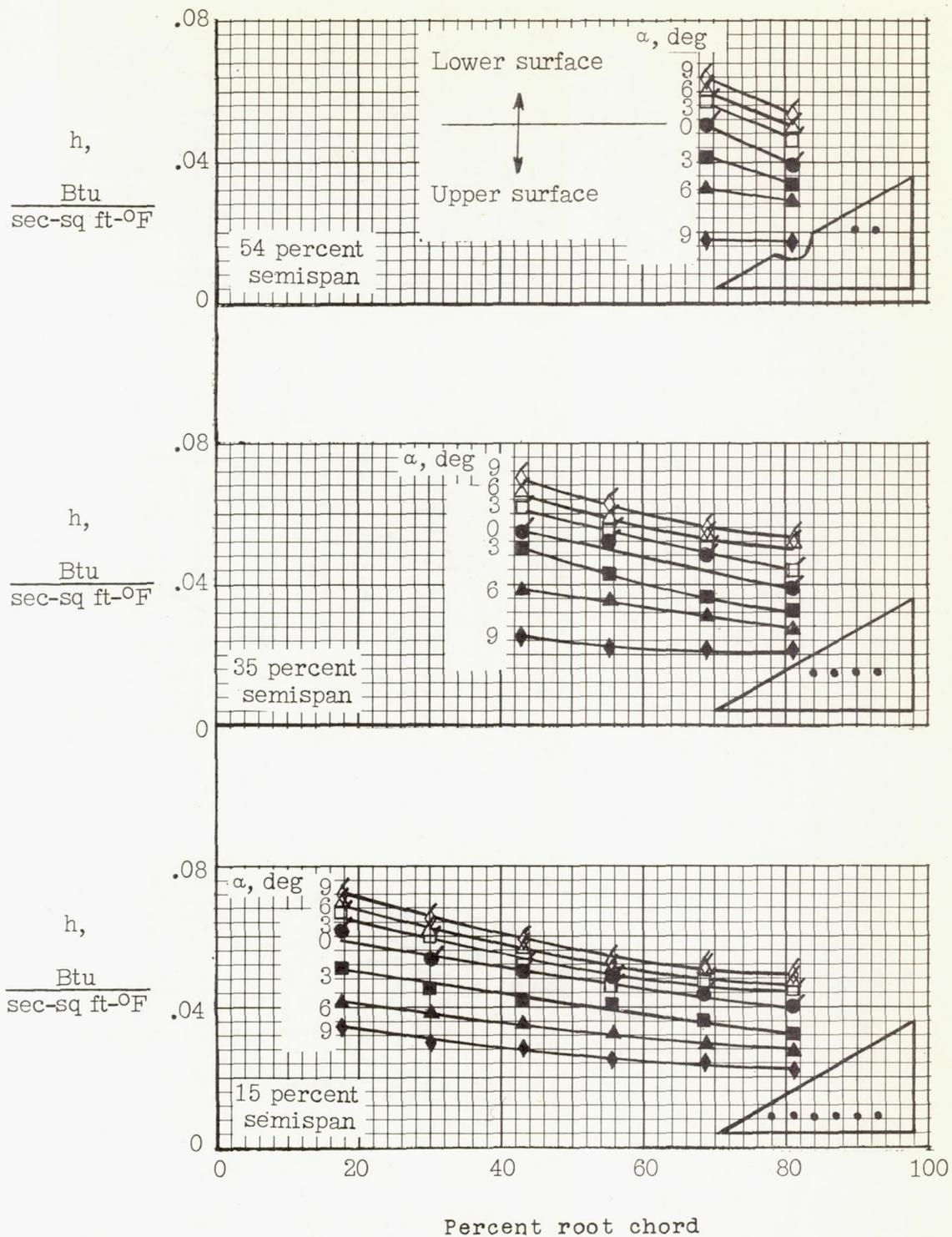Figure 5.- Variation of pressure coefficient with angle of attack for the 12 measuring stations.
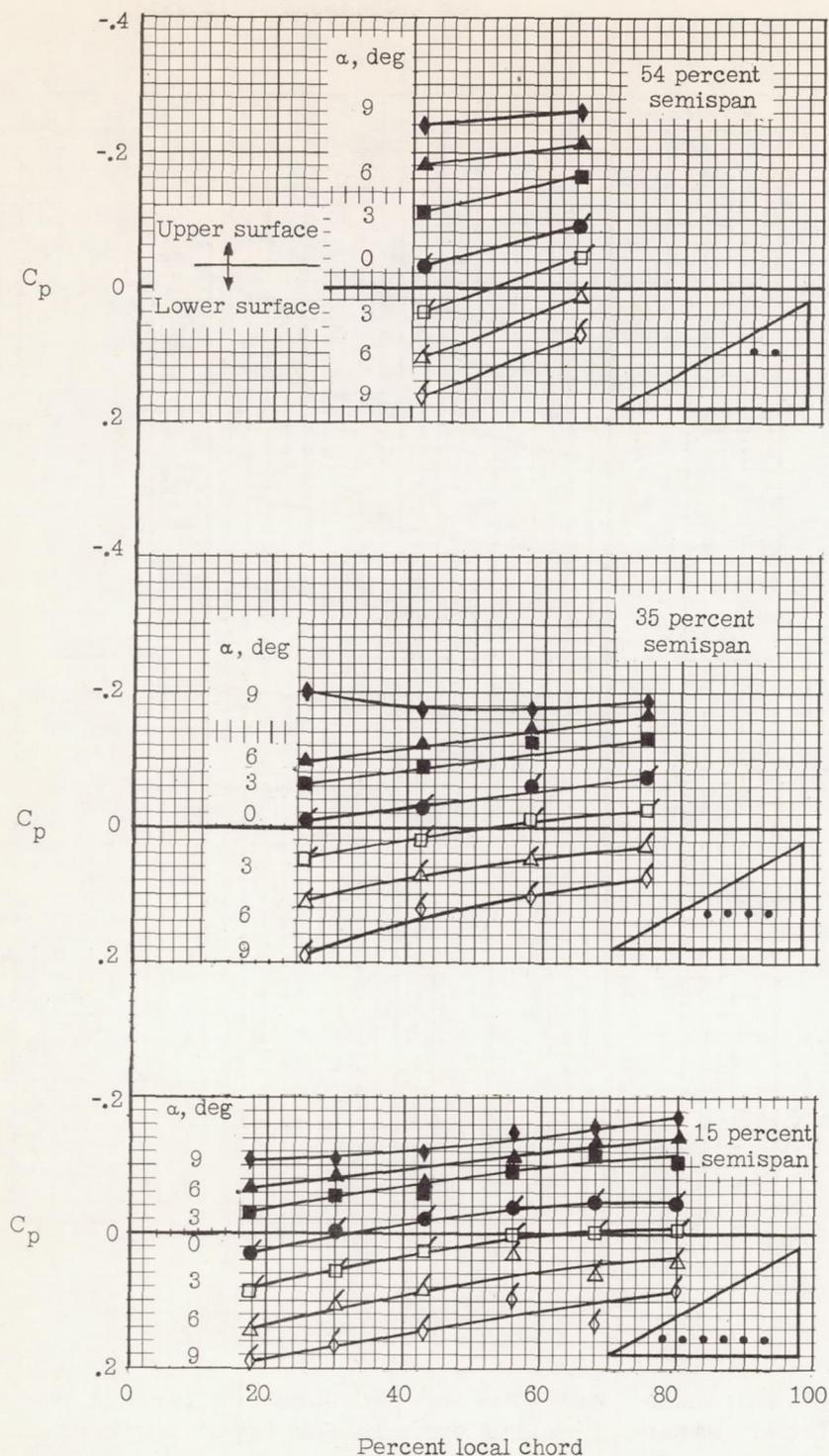
Figure 6.- Variation of pressure coefficient along the three semispan stations for four angles of attack. (Solid symbols for upper surface, flagged symbols for lower surface.)
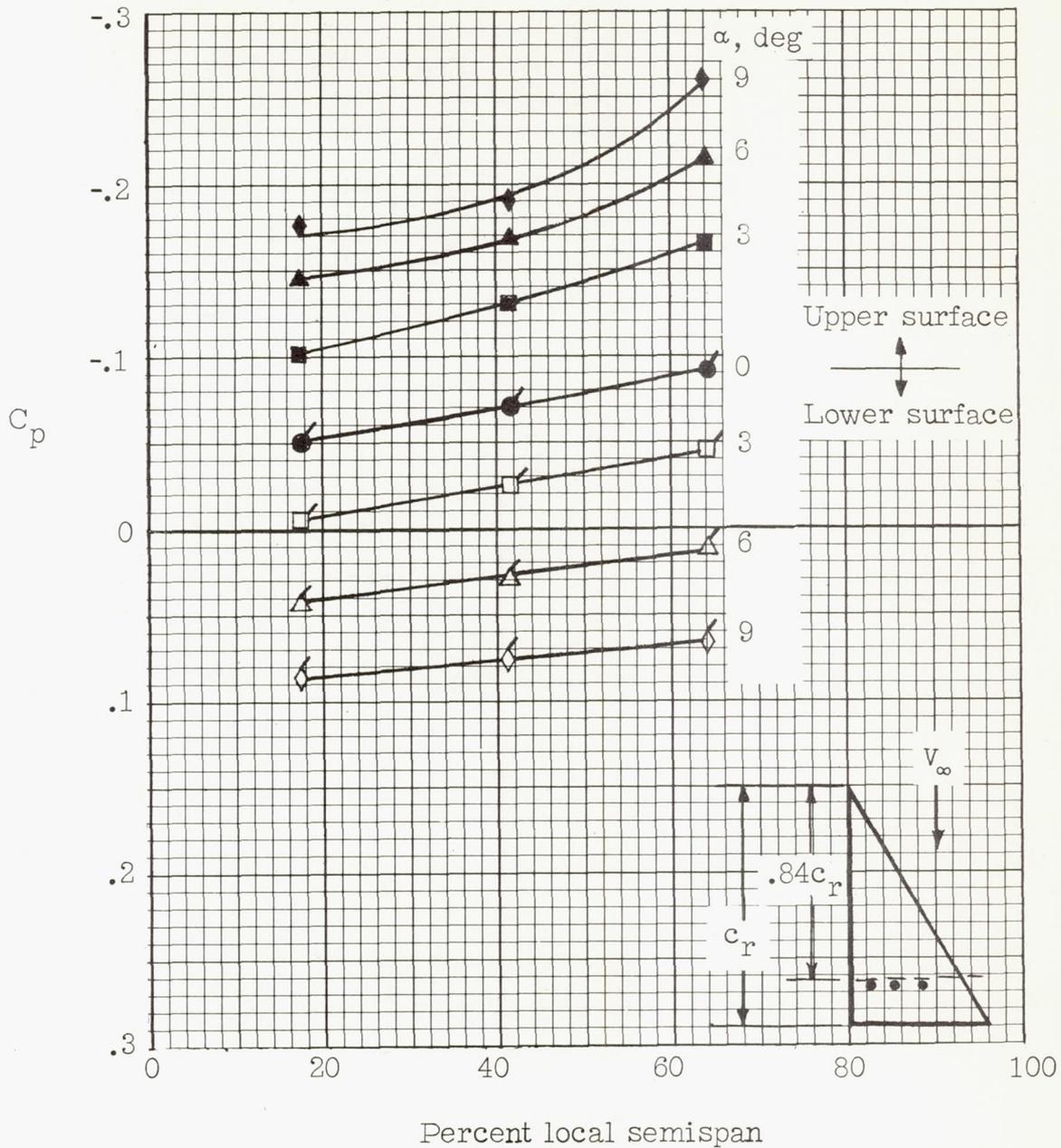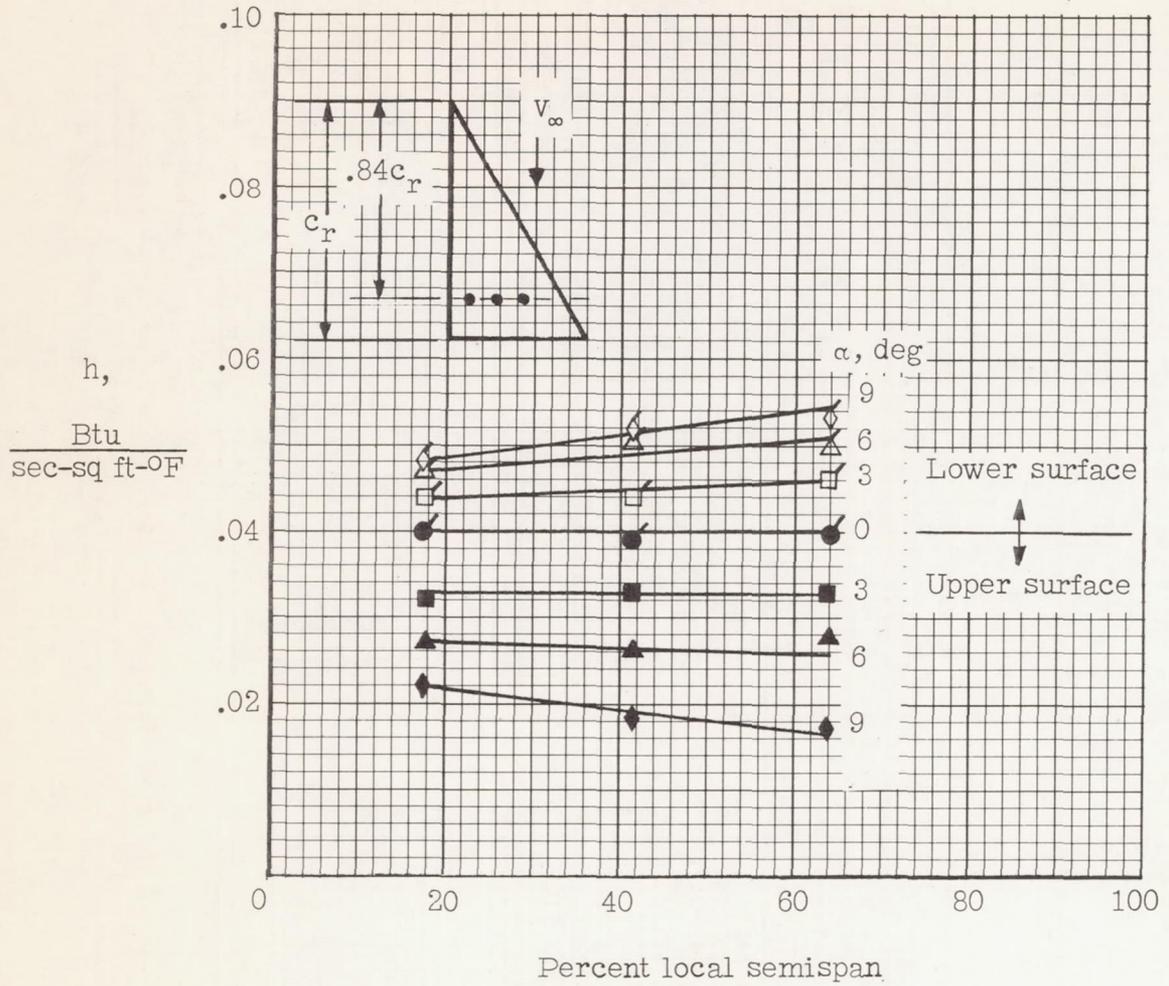
Figure 7.- Spanwise variation of pressure coefficient at $0.84c_r$ for four angles of attack. (Solid symbols for upper surface, flagged symbols for lower surface.)
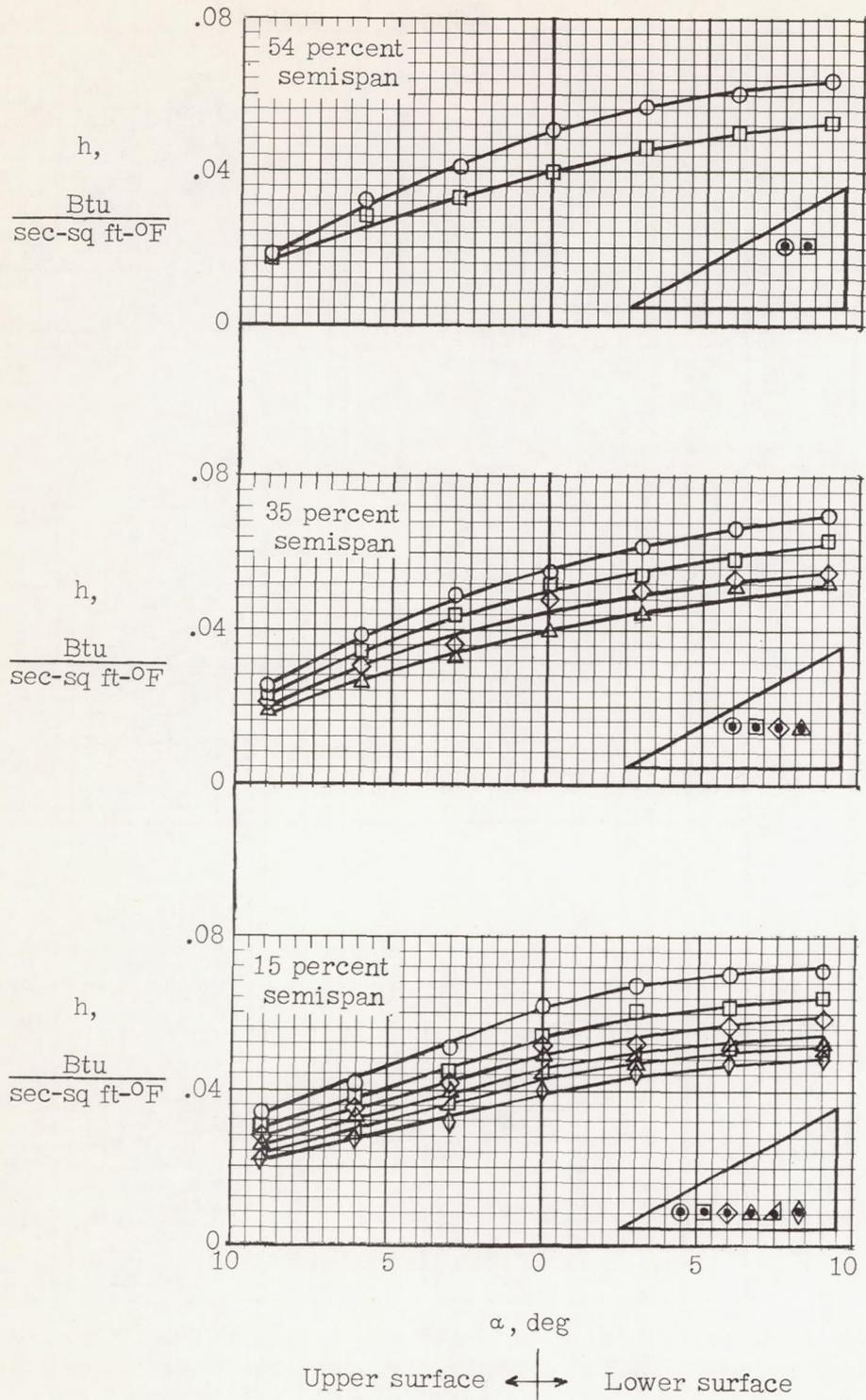
Figure 8.- Variation of heat transfer coefficient with angle of attack
for the 12 measuring stations.

Figure 9.- Chordwise variation of heat transfer coefficient along the three semispan stations for four angles of attack. (Solid symbols for upper surface, flagged symbols for lower surface.)

Figure 10.- Spanwise variation of heat transfer coefficient at $0.84c_r$ for four angles of attack. (Solid symbols for upper surface, flagged symbols for lower surface.)
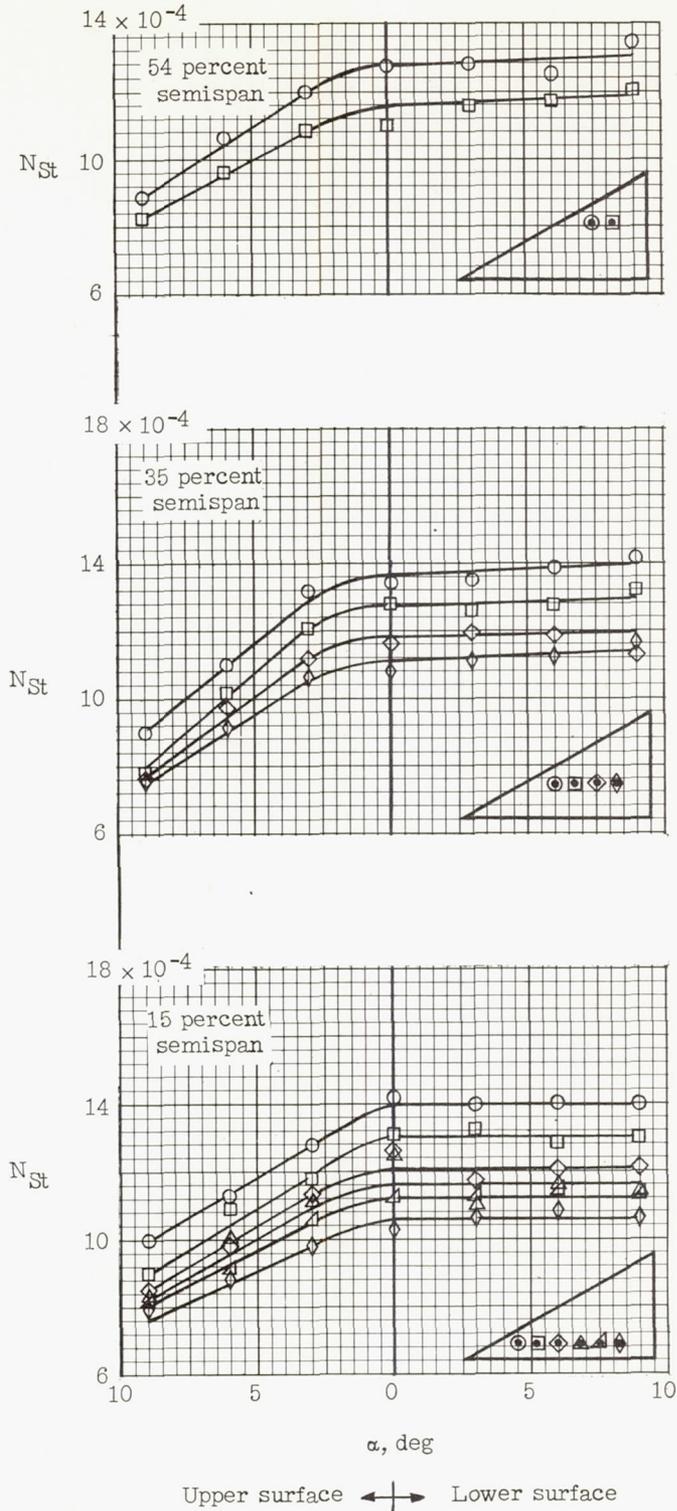
Figure 11.- Variation of Stanton number with angle of attack for the
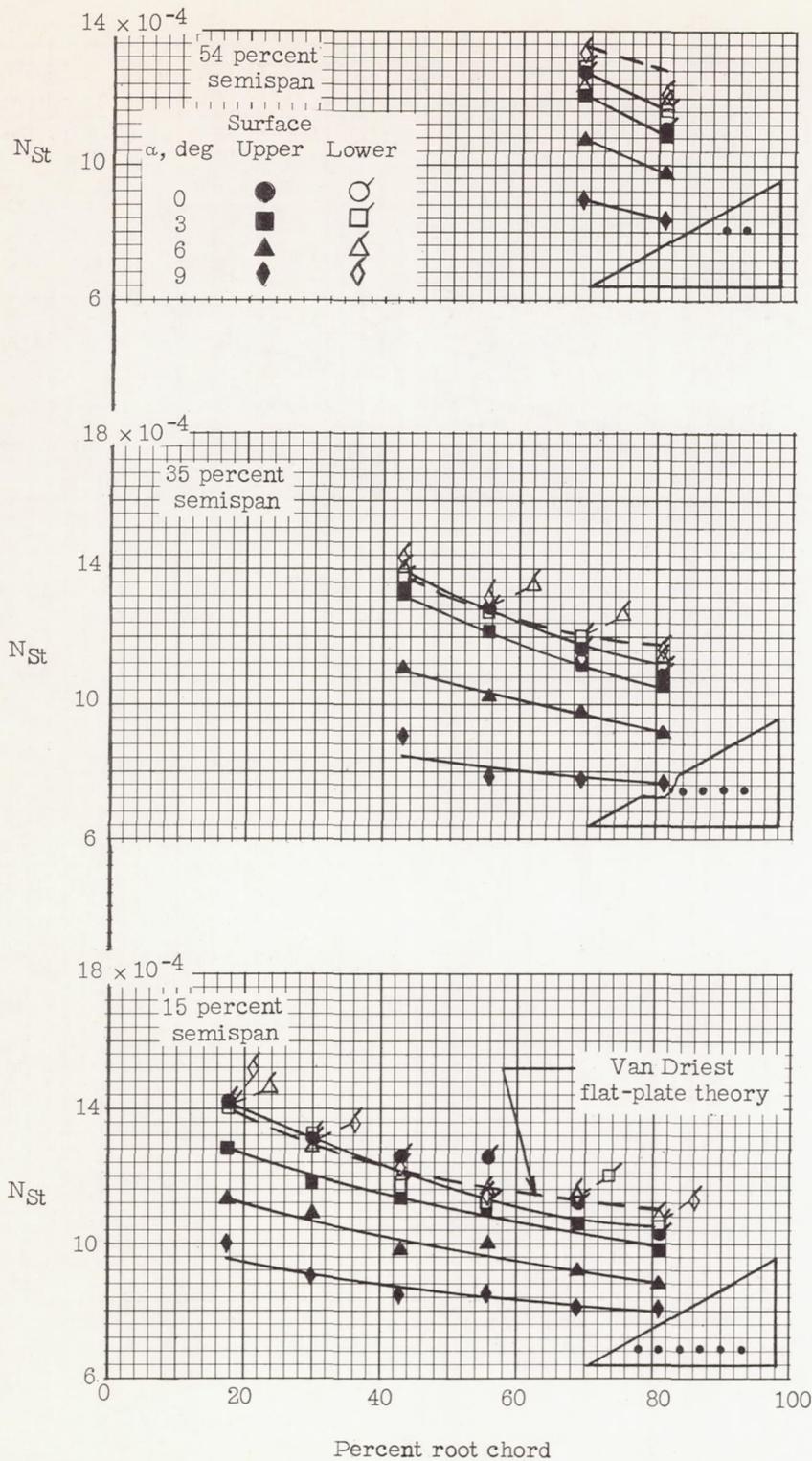12 measuring stations.

Figure 12.- Chordwise variation of Stanton number along the three semi-span stations for four angles of attack.
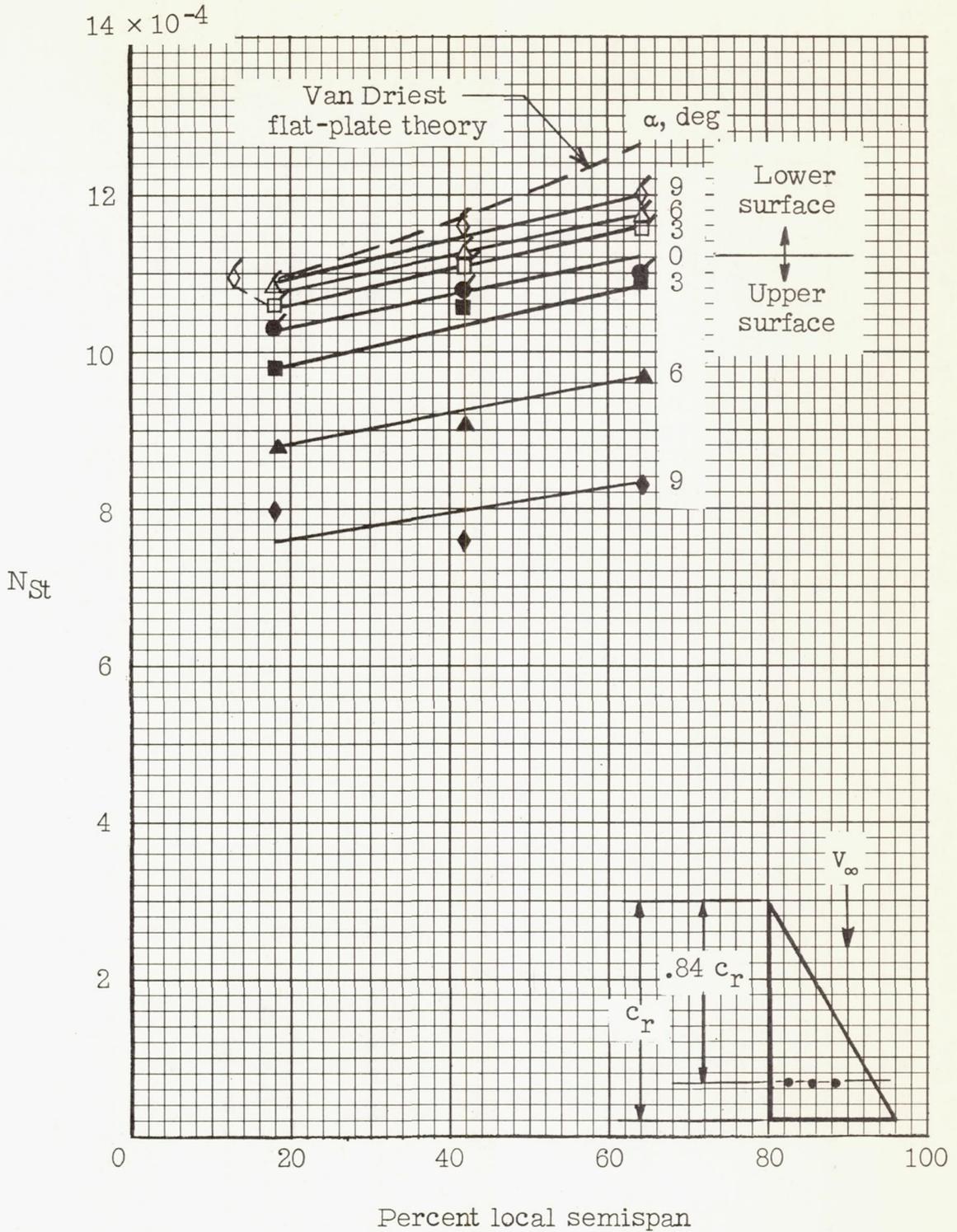
Figure 13.- Spanwise variation of Stanton number at 0.84c_r for four
angles of attack.